Supporting Information

Phosphorous Diffusion Through Ni_2P — Low Energy Diffusion Path and its Unique Local Structure

José Contreras-Mora [1,2], Hiroko Ariga-Miwa,[1] Satoru Takakusagi[1], Christopher T. Williams [2], Kiyotaka Asakura* [1]*

[1] Institute for Catalysis, Hokkaido University, Kita 21-10 Kita, Sapporo 001-0021, Japan

[2] Department of Chemical Engineering, University of South Carolina, Columbia 29208, SC, USA

**** corresponding authors: WILLIA84@csc.sc.edu, askr@cat.hokudai.ac.jp***

1. **The coordinates derived from DFT calculations in perfect crystal**

2. **Lattice parameter comparison**

3. **Calculated and experimental distances of Ni-P and P-P**

4. **Displacements of Ni from the calculated perfect structure**

5. **P-P distances in $I^{P}_{1\rightarrow1}$, $I^{P}_{2\rightarrow2}$ intermediate structure**

6. **Some diffusion pathway.**

7. **Ni_2P structure and Displacement during the diffusion process.**

8. **Partial density of states (PDOS) for a) Ni and b) P**

1. The coordinates derived from DFT calculations in perfect crystal

Table S1 shows the calculated coordinates of Ni and P in perfect crystal.

Table S1 coordinates of Ni and P in perfect crystal derived from the calculation.

	X	Y	Z		X	Y	Z
Ni1	1.53	0.00	0.00	Ni17	-1.77	7.13	1.69
Ni2	2.18	3.77	0.00	Ni18	1.17	8.17	1.69
Ni3	5.12	1.33	0.00	Ni19	4.48	5.10	0.00
Ni4	3.55	0.00	1.69	Ni20	5.12	8.87	0.00
Ni5	1.17	2.03	1.69	Ni21	-3.71	6.43	0.00
Ni6	4.12	3.07	1.69	Ni22	6.49	5.10	1.69
Ni7	7.42	0.00	0.00	Ni23	4.12	7.13	1.69
Ni8	8.07	3.77	0.00	Ni24	-4.72	8.17	1.69
Ni9	-0.77	1.33	0.00	Ni25	1.53	0.00	3.37
Ni10	9.44	0.00	1.69	Ni26	2.18	3.77	3.37
Ni11	7.06	2.03	1.69	Ni27	5.12	1.33	3.37
Ni12	-1.77	3.07	1.69	Ni28	3.55	0.00	5.06
Ni13	-1.41	5.10	0.00	Ni29	1.17	2.03	5.06
Ni14	-0.77	8.87	0.00	Ni30	4.12	3.07	5.06
Ni15	2.18	6.43	0.00	Ni31	7.42	0.00	3.37
Ni16	0.60	5.10	1.69	Ni32	8.07	3.77	3.37
Ni33	-0.77	1.33	3.37	Ni51	5.12	1.33	6.74
Ni34	9.44	0.00	5.06	Ni52	3.55	0.00	8.43

Ni35	7.06	2.03	5.06	Ni53	1.17	2.03	8.43
Ni36	-1.77	3.07	5.06	Ni54	4.12	3.07	8.43
Ni37	-1.41	5.10	3.37	Ni55	7.42	0.00	6.74
Ni38	-0.77	8.87	3.37	Ni56	8.07	3.77	6.74
Ni39	2.18	6.43	3.37	Ni57	-0.77	1.33	6.74
Ni40	0.60	5.10	5.06	Ni58	9.44	0.00	8.43
Ni41	-1.77	7.13	5.06	Ni59	7.06	2.03	8.43
Ni42	1.17	8.17	5.06	Ni60	-1.77	3.07	8.43
Ni43	4.48	5.10	3.37	Ni61	-1.41	5.10	6.74
Ni44	5.12	8.87	3.37	Ni62	-0.77	8.87	6.74
Ni45	-3.71	6.43	3.37	Ni63	2.18	6.43	6.74
Ni46	6.49	5.10	5.06	Ni64	0.60	5.10	8.43
Ni47	4.12	7.13	5.06	Ni65	-1.77	7.13	8.43
Ni48	-4.72	8.17	5.06	Ni66	1.17	8.17	8.43
Ni49	1.53	0.00	6.74	Ni67	4.48	5.10	6.74
Ni50	2.18	3.77	6.74	Ni68	5.12	8.87	6.74
Ni69	-3.71	6.43	6.74	P15	0.00	0.00	5.06
Ni70	6.49	5.10	8.43	P16	5.89	3.40	3.37
Ni71	4.12	7.13	8.43	P17	8.83	1.70	3.37
Ni72	-4.72	8.17	8.43	P18	5.89	0.00	5.06
P1	0.00	3.40	0.00	P19	-2.94	8.50	3.37
P2	2.95	1.70	0.00	P20	0.00	6.80	3.37

P3	0.00	0.00	1.69	P21	-2.94	5.10	5.06
P4	5.89	3.40	0.00	P22	2.94	8.50	3.37
P5	8.83	1.70	0.00	P23	5.89	6.80	3.37
P6	5.89	0.00	1.69	P24	2.94	5.10	5.06
P7	-2.95	8.50	0.00	P25	0.00	3.40	6.74
P8	0.00	6.80	0.00	P26	2.94	1.70	6.74
P9	-2.95	5.10	1.69	P27	0.00	0.00	8.42
P10	2.94	8.50	0.00	P28	5.89	3.40	6.74
P11	5.89	6.80	0.00	P29	8.83	1.70	6.74
P12	2.94	5.10	1.69	P30	5.89	0.00	8.42
P13	0.00	3.40	3.37	P31	-2.94	8.50	6.74
P14	2.94	1.70	3.37	P32	0.00	6.80	6.74
P33	-2.95	5.10	8.42	P35	5.89	6.80	6.74
P34	2.94	8.50	6.74	P36	2.94	5.10	8.42

2. Lattice parameter comparison

Table S2 show the lattice parameters from previous DFT and experimental studies. The lattice parameters of present study are in good agreement with those values.

Table S2: Comparison of calculated and experimental lattice parameters.

Functional	a=b/Å	c/Å	Reference
CC2	5.859	3.382	1
DF-GGA	5.855	3.339	2
GGA	5.88	3.37	3
Experimental	5.87	3.39	4
GGA	5.89	3.37	This work

3. Calculated and experimental distances of Ni-P and P-P

Table S3 shows the calculated and experimental distances of Ni and P for the two local structures, tetrahedral and square-base pyramid. Diffusion barrier calculations were obtained using cNEB [5] for the transient state $TS^{P}_{2\rightarrow1}$ and intermediate state $I^{P}_{1\rightarrow2}$ and are illustrated in **Figure S1** with the corresponding pathways. This figure suggests how the P diffuses in both $TS^{P}_{2\rightarrow1}$ (Arabic numbers) and $I^{P}_{1\rightarrow2}$ (roman numbers. For $TS^{P}_{2\rightarrow1,}$ the P (2) (red dot for better display) moves from the lattice site to different interstitial sites within Ni_3P, therefore forming a vacancy V^{P}_{2}. Then, after the transient state "mountain", the P (2) goes to the vacancy V^{P}_{1} site in Ni_3P_2. Nonetheless, for the diffusion path of the intermediate state $I^{P}_{1\rightarrow2,}$ it can be observed that the P (1) (red dot) goes from the lattice site in Ni_3P_2 down to Ni_3P until it reaches the interstitial site in Ni_3P ($I^{P}_{1\rightarrow2}$), and since the difference between the "valley" (intermediate state) and the "mountain" (next point) is only 0.008 eV, the P (1) can then diffuse to the V^{P} site. These diffusion pathways and diffusion barriers provide good evidence that the $I^{P}_{1\rightarrow2}$ might be the only possible path and therefore its relative energy is significantly lower than the $TS^{P}_{2\rightarrow1}$ and the other intermediate states.

Table S3: Comparison of calculated and experimental Ni-P and P-P distances for tetrahedral and Square-base pyramid structures

Local Structures	Parameters	Calculated / Å	Experimental / Å*
	Ni (1)-P (1)	2.21	2.21
	Ni (1)-P (2)	2.28	2.27
Tetrahedral	P (1)-P (1)	3.40	3.38
	P (2)-P (2)	3.37	3.38
	P (1)-P (2)	3.80	3.78
	Ni (2)-P (2)	2.34	2.37
	Ni (2)-P (1)	2.47	2.48
Square-base pyramid	P (2)-P (1)	3.80	3.78
	P (1)- P (1)	3.40	3.38

4. Displacements of Ni from the calculated perfect structure

Table S4 shows the difference in position of Ni with respect to the perfect structure. The equation used to calculate the displacements in Å is as follow:

$$\sqrt{(X_1 - X_2)^2 + (Y_1 - Y_2)^2 + (Z_1 - Z_2)^2} \quad \text{(S1)}$$

where, X_1, Y_1 and Z_1 are the position for the perfect structure, and X_2, Y_2 and Z_2 are the position for V^P_1, V^P_2, $I^P_{1\rightarrow 2}$ and $TS^P_{2\rightarrow 1}$.Ni displacements were significant (<0.1 Å) for all of the structures studied, except for V^P_2.

Table S4: Ni displacement for the different vacancies

	Displacement(Å)			
Ni #	V^P_1	V^P_2	$I^P_{1\rightarrow 2}$	$TS^P_{2\rightarrow 1}$
Ni_{16}(2)	0.13	0.04	0.11	0.14
Ni_{17}(2)	0.13	0.02	0.11	0.13
Ni_{18}(2)	0.13	0.01	0.11	0.20
Ni_{37}(1)	0.06	0.03	0.19	0.06
Ni_{38}(1)	0.06	0.03	0.19	0.11
Ni_{39}(1)	0.06	0.08	0.19	0.20
Ni_{40}(2)	0.13	0.08	0.38	1.18
Ni_{41}(2)	0.13	0.02	0.38	0.12
Ni_{42}(2)	0.13	0.01	0.38	0.32
Ni_{61}(1)	0.01	0.03	0.19	0.16
Ni_{62}(1)	0.01	0.03	0.19	0.05
Ni_{63}(1)	0.01	0.08	0.19	0.06
Ni_{64}(2)	0.03	0.04	0.11	0.15
Ni_{65}(2)	0.03	0.02	0.11	0.14
Ni_{66}(2)	0.03	0.01	0.11	0.10

5. P-P distances in $l^{P}_{1\rightarrow1,}$ $l^{P}_{2\rightarrow2}$ intermediate structure

Table S5 shows the summary of P-P distances in $l^{P}_{1\rightarrow1,}$ $l^{P}_{2\rightarrow2}$ intermediate structure.

Table S5: Summary of P-P distances of the in-plane ($l^{P}_{1\rightarrow1,}$ $l^{P}_{2\rightarrow2}$) intermediate diffusion. Red P represent the diffusive atom. For $l^{P}_{1\rightarrow1}$ the vacancy is on P_{20} (1), while for $l^{P}_{2\rightarrow2}$ is P_{24} (2).

Ni Reference	P-P	$l^{P}_{1\rightarrow1}$ / Å	P-P	$l^{P}_{2\rightarrow2}$ / Å
	P_{13} (1')-P_{21} (2)	3.78	P_{13} (1)-P_{21} (2')	3.83
Ni_{37} (1)	P_{13} (1')-P_{9} (2)	3.76	P_{13} (1)-P_{9} (2)	3.84
	P_{21} (2)-P_{9} (2)	3.44	P_{21} (2')-P_{9} (2)	3.37
	P_{24} (2)-P_{25} (1)	3.78	P_{25} (1)-P_{13} (1)	3.35
	P_{24} (2)-P_{32} (1)	3.78	P_{25} (1)-P_{32} (1)	3.49
	P_{24} (2)-P_{13} (1')	3.20	P_{20} (2)-P_{32} (1)	4.80
Ni_{40} (2)	P_{25} (1)-P_{13} (1')	3.76	P_{21} (2')-P_{32} (1)	2.41
	P_{25} (1)-P_{32} (1)	3.43	P_{21} (2')-P_{20} (1)	2.41
	P_{32} (1)-P_{13} (1')	3.75	P_{21} (2')-P_{13} (1)	3.96
	--	--	P_{21} (2')-P_{25} (1)	3.96

6. Some diffusion pathway.

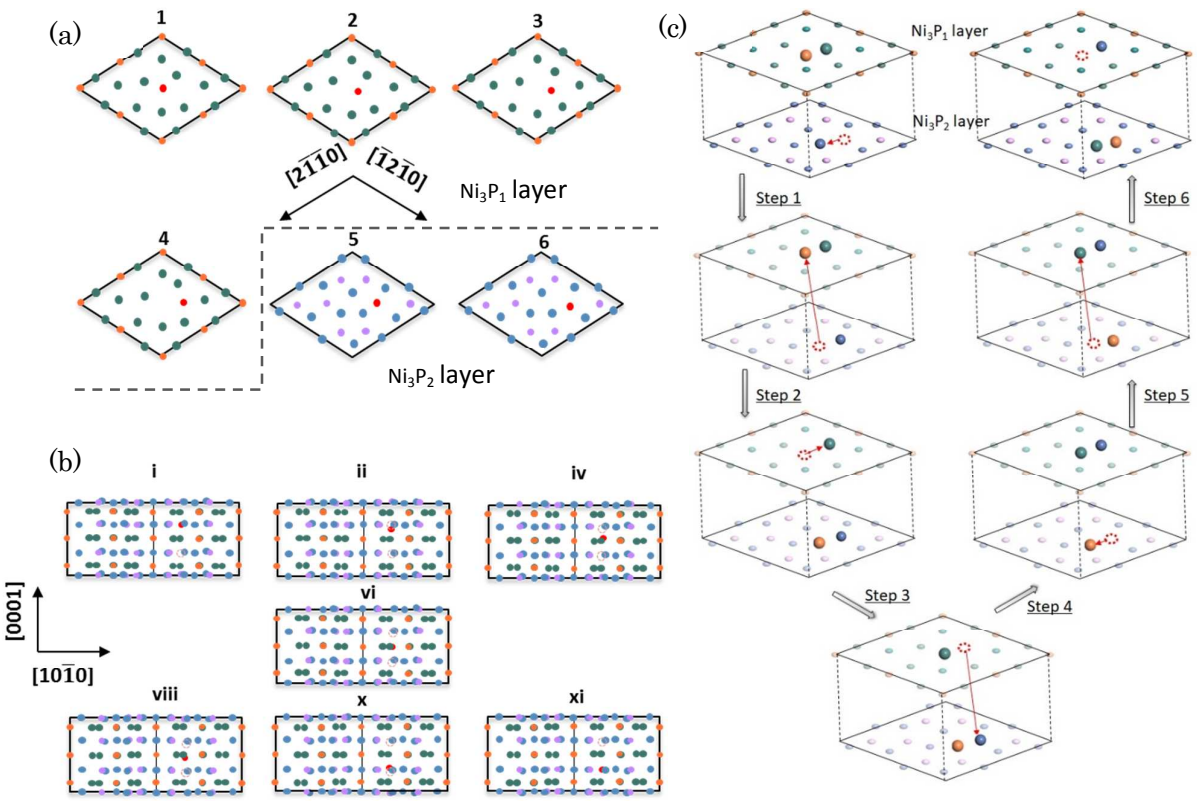

(d)

Structure	Relative energy / eV
1 (V^P_1)	0.00
2	0.57
3	1.20
4	2.28
5	1.51
6	1.91
7 (V^P_2)	0.20

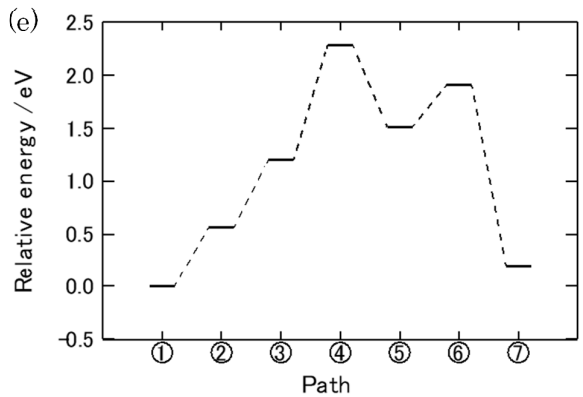

Figure S1: Diffusion Pathways for $TS^P_{2\rightarrow1}$ (a) and $I^P_{1\rightarrow2}$ (b) Arabic numbers represent the points and diffusion path of $TS^P_{2\rightarrow1}$, Roman number indicates the points and diffusion path of $I^P_{1\rightarrow2}$ and the red dotted atom represents the diffusive phosphorous for both structures. Layers change from Ni_3P_1 to Ni_3P2 between 4 and 5 in the Figure S1(a) (c) shows the "six-jump cycle mechanism" (d) and (e)shows the relative energy of each step of the "six-jump cycle mechanism".

7. Ni_2P structure and Displacement during the diffusion process.

Figure S2 the perfect structure supercell with the square-base pyramid and the tetrahedral local structures. Also, it shows the zoom in of the different Ni and P that are affected by V^P_1, $I^P_{1\rightarrow 2}$ and $TS^P_{2\rightarrow 1}$. **Figure S2a** shows the two local structures and some of the neighbor Ni and P from the 2nd layer to the 5th of the perfect structure. **Figure S2b** illustrates substantial displacements of Ni atoms at $Ni_{16\text{-}18}$ (2) and $Ni_{40\text{-}42}$ (2) (both in Ni_3P), which move downward and upward, respectively, from the vacancy V^P_1. Likewise, **Figure S2c** shows Ni displacement, but now for $I^P_{1\rightarrow 2}$. For this intermediate step, $Ni_{16\text{-}18}$ (2) move downward away from the vacancy (as we saw with V^P_1), but as a result of the P_{32} (1') diffusion, $Ni_{40\text{-}42}$ (2) moves away in the same layer, to make space for P_{32} (1'). Also, at the same time $Ni_{64\text{-}66}$ (2) moves upward away from the other vacancy $V^P_{1'}$. $Ni_{37\text{-}39}$ (1) move upward, and $Ni_{61\text{-}63}$ (1) downward, both toward the diffused P_{32} (1').

For $TS^P_{2\rightarrow 1}$ (**Figure S2d**) shows that the diffusion makes some local distortions. Thanks to the P_{24} (2) diffusion, the P_{32} (1) bonding with Ni_{40} (2) breaks. Basically, the Ni_{40} moves upward, but at the same time P_{32} moves upward as well. The phosphorous diffusion and the vacancy makes the local structure becomes a trigonal pyramidal. The P_{24} (2) surrounding Ni ($Ni_{40\text{-}42}$) move upward

and away of the diffused phosphorous. $Ni_{16\text{-}18}$ moves downward away of the vacancy, and $Ni_{64\text{-}66}$ move upwards. The only Ni on the fifth layer is Ni_{61}.

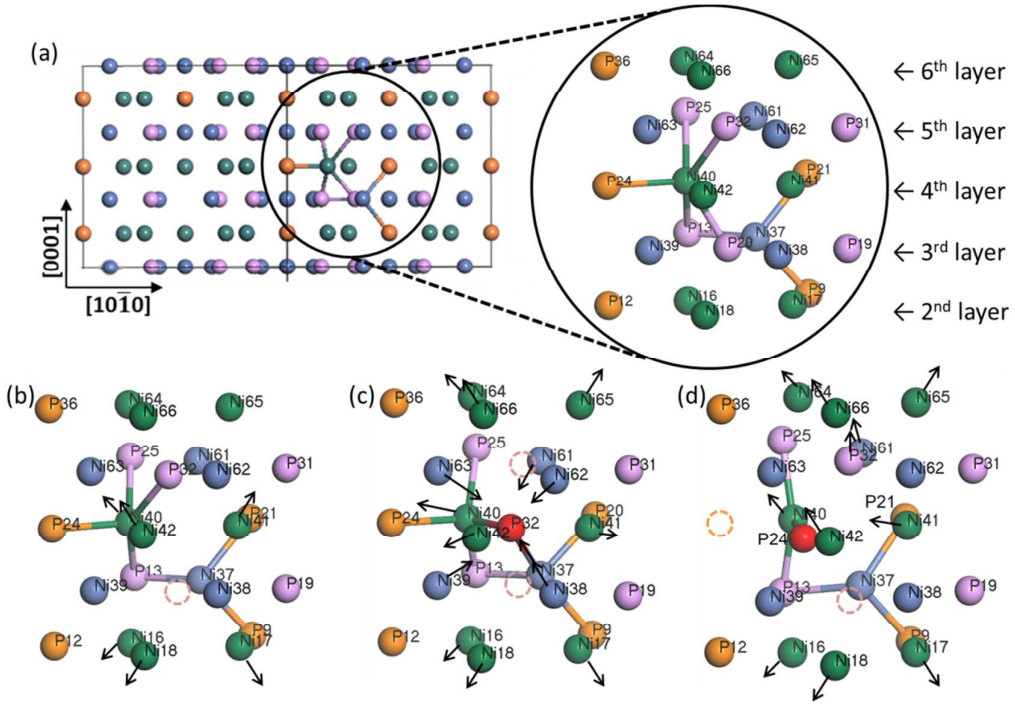

Figure S2: a) Perfect structure supercell and a zoom in for the Ni and P near the tetrahedral and square-base pyramid structures, b) Ni displacement in V^{P}_{1}, c) $I^{P}_{1\rightarrow 2}$ and d) for $TS^{P}_{2\rightarrow 1}$. Pink and orange doted circles represent vacancy V^{P}_{1} and V^{P}_{2}, black arrows represent the Ni displacements and the red P represent the diffusion phosphorous.

8. Partial density of states (PDOS) for a) Ni and b) P

Figure S3 shows the partial density of states (PDOS) for a) Ni and b) P. The d band consist mostly of Ni_{3d} (**Fig. S3b**), but also some of P_{3p} (**Fig. S3a**) and it is found from 1.3 to -4 eV, the delocalized band composed with P_{3p} and Ni_{3d} located from around -5 to -9 eV and the phosphorous s band (**Fig. S3b**) from around -11 to -15 eV. Overall, the main d band contribution comes from the Ni.

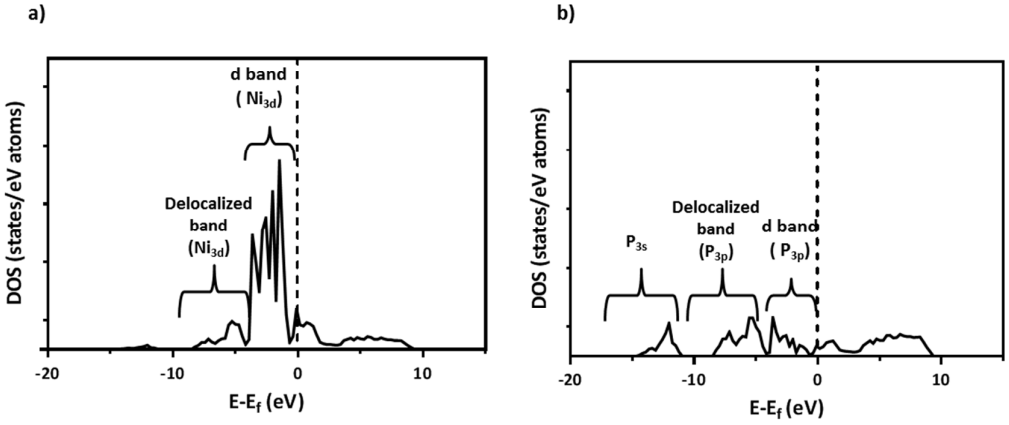

Figure S3: PDOS for a) Nickel and b) Phosphorous with the corresponding bands.

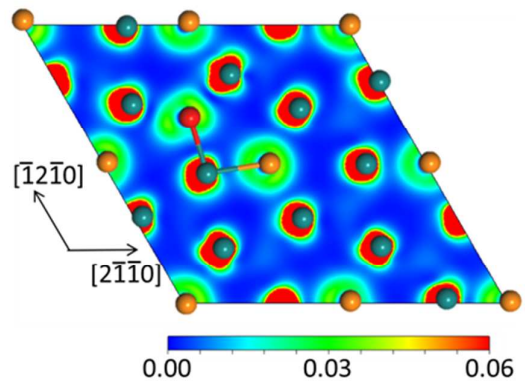

Figure S4: Electron density distribution of $I^{P}_{1\rightarrow 2}$ structure for the energy range of -0.6 – 0eV.

References

(1) Kanama, D.; Oyama, S. T.; Otani, S.; Cox, D. F. Photoemission and LEED Characterization of Ni2P(0 0 0 1). *Surf. Sci.* **2004**, *552* (1–3), 8–16.

(2) Rodriguez, J. A.; Kim, J.-Y.; Hanson, J. C.; Sawhill, S. J.; Bussell, M. E. Physical and Chemical Properties of MoP, Ni2P, and MoNiP Hydrodesulfurization Catalysts: Time-Resolved X-Ray Diffraction, Density Functional, and Hydrodesulfurization Activity Studies. *J. Phys. Chem. B* **2003**, *107* (26), 6276–6285.

(3) Li, Q.; Hu, X. First-Principles Study of Ni2P (0001) Surfaces. *Phys. Rev. B* **2006**, *74* (3), 35414.

(4) Rundqvist, S. X-Ray Investigations of Mn3p, Mn2p, and Ni2p. *Acta Chem. Scand.* **1962**, *16* (4), 992-.

(5) Zarkevich, N. A.; Johnson, D. D. Nudged-Elastic Band Method with Two Climbing Images: Finding Transition States in Complex Energy Landscapes a). *J. Chem. Phys.* **2015**, *142* (2), 24106.